



Research Report

Pore-expansion of Highly Monodispersed Mesoporous Silica Spheres and Application to the Synthesis of Porous Ferromagnetic Composites

Mamoru Mizutani, Yuri Yamada, Tadashi Nakamura and Kazuhisa Yano

Report received on Apr. 10, 2012

■ABSTRACT■ We report on the synthesis of pore-expanded monodispersed mesoporous silica spheres (MMSS) and ferromagnetic mesoporous composites. Pore-expansion of MMSS was achieved using two different solvothermal methods; a surfactant exchange method, in which surfactant molecules inside the mesopores were exchanged for those with longer alkyl-chain lengths, and a swelling agent incorporation method, by which swelling agents such as various hydrocarbons were incorporated into the mesopores. The mesopores were expanded up to two to three times the original value (3.7 and 5.5 nm using the respective methods) without any modification to the uniform spherical shape and radial alignment of the hexagonally-ordered mesopores. FePt-MMSS composites were also successfully prepared by synthesizing FePt nanoparticles inside the mesopores of the pore-expanded MMSS. The composites exhibited ferromagnetic behavior at room temperature and retained sufficient mesoporosity to incorporate various chemicals, nanoparticles, quantum dots, enzymes, and DNA molecules. The FePt-MMSS composites are expected to have potential applications in drug delivery systems, gene delivery systems, magnetic hyperthermia devices, and magnetic photonic crystals.

■KEYWORDS■ Mesoporous Silica, Pore-expansion, Surfactant, Expander, Post-synthesis, Solvothermal, FePt

1. Introduction

The discovery of an ordered mesoporous silica, MCM-41, in the early 1990s by Mobil researchers⁽¹⁾ has been followed by extensive studies by many researchers to date.⁽²⁾ Many studies on the synthesis of ordered mesoporous silicas have been conducted for applications such as new types of catalysts,⁽³⁾ adsorbents,⁽⁴⁾ and host materials.⁽⁵⁾ Morphological control of these materials has been one of the major challenges required to realize their industrial applications. Micrometer-size nonporous monodispersed silica spheres were first synthesized in 1968 by Stöber using a water/alcohol/ammonia/tetraalkoxysilane system.⁽⁶⁾ This method has been modified by the addition of cationic surfactants and/or by the use of other organic solvents for the synthesis of mesoporous silica spheres.⁽⁷⁾

We have successfully synthesized highly monodispersed mesoporous silica spheres (MMSS) with hexagonally-ordered mesostructures using *n*-alkyltrimethylammonium bromide as a surfactant template.⁽⁸⁾ MMSS are useful for fundamental research on mesoporous materials, because the uniform size of MMSS enables the catalytic activity or diffusion kinetics in the mesopore channels to be analyzed

without the effect of particle size. An alternative application of MMSS is to colloidal photonic crystals, and we have already demonstrated the fabrication of various types of colloidal crystals using MMSS and their derivative composites as building blocks.⁽⁹⁾

The pore diameter of the MMSS can be tuned by changing the alkyl chain lengths of the surfactant.⁽¹⁰⁾ However, the maximum pore diameter of MMSS is 2.5 nm. Therefore, expansion of the pores in MMSS is of considerable importance, because large-pore MMSS are promising for new types of colloidal crystals obtained by the incorporation of large molecules, such as metal complexes and biomolecules. Various methods have been attempted to expand the pore diameter of mesoporous materials. The most common technique is the introduction of a swelling agent into the structure-directing template, either in the preparation step,⁽¹¹⁾ or during post-hydrothermal treatment.⁽¹²⁾ The pore diameter can be easily expanded using these methods; however, little attention has been paid to preservation of the morphology.

We have attempted to directly synthesize pore-expanded MMSS using swelling agents such as dococyltrimethylammonium chloride (C₂₂TMACl) and 1,3,5-trimethylbenzene (TMB). However, despite variations of the synthesis conditions, such as the

concentration and ratio of the surfactant and silica source, and the type and fraction of solvent, monodispersed particles have not been obtained. Therefore, we have pursued a new method to achieve pore expansion of MMSS while retaining spherical morphology, high monodispersity, and radial alignment of the hexagonally-ordered mesopores.

FePt with an ordered face-centered tetragonal (fct) phase has attracted much attention as a material that exhibits high magnetocrystalline anisotropy (K_1 : 6.6 MJ m^{-3}), saturation magnetization (M_s : 1140 emu cm^{-3}),⁽¹³⁾ and relatively high chemical stability. FePt nanoparticles have potential applications in data storage, permanent magnetic nanocomposites, and biomedicines.⁽¹⁴⁾ However, it is generally difficult to handle FePt nanoparticles due to their tendency to readily aggregate. The incorporation of FePt nanoparticles into the mesopores of MMSS is promising, not only to avoid aggregation of the nanoparticles, but also to achieve ease of handling. However, FePt nanoparticles only exhibit ferromagnetism when their diameters are greater than 2.8–3.3 nm,⁽¹⁵⁾ therefore, it is necessary to use mesoporous silica with larger pore diameters.

In this paper, we report on the pore expansion of MMSS using both a surfactant exchange (SE) method and a swelling agent incorporation (SI) method. We discuss the mechanism of the pore-expansion process for each method. In addition, the incorporation of ferromagnetic FePt nanoparticles into the pore-expanded MMSS is described.

There is a variety of possible applications for MMSS materials, and the methods described here are very important for the incorporation of large molecules such as metal complexes and proteins into the mesopores, for the size control of nanoparticles inside the mesopores, and for the retention of pore space after the grafting of organic functional groups.

2. Experimental Section

2.1 Chemicals

N-alkyltrimethylammonium bromide or chloride ($C_n\text{TMABr}$ or $C_n\text{TMACl}$, $n = 10, 14, 18, 22$), tetramethyl orthosilicate (TMOS), 1 M NaOH solution, ethanol (EtOH), methanol (MeOH), distilled water and other pore-expansion reagents used were the highest grade available and were used without further purification.

2.2 Synthesis of MMSS n ($n = 10, 14, 18$)

MMSS n ($n = 10, 14, 18$) silica/surfactant composites were prepared by a surfactant-templating method using $C_{10}\text{TMABr}$, $C_{14}\text{TMACl}$, or $C_{18}\text{TMACl}$ as respective templating agents.^(8,9) In a typical synthesis procedure of MMSS18, $C_{18}\text{TMACl}$ (3.83 g) and 1 M NaOH solution (2.28 mL) were dissolved in a methanol–water (60:40 w/w) solution (800 g). TMOS (1.32 g) was added to the solution with vigorous stirring at 25°C and the solution was continuously stirred for 8 h, after which the mixture was aged overnight. A white powdered sample was obtained by repeated filtration and washing with distilled water, followed by drying at 45°C for 72 h. The template surfactant molecules inside MMSS18 were not removed before the pore-expanding process.

2.3 Synthesis of MMSS22 by the SE Method

MMSS22 silica/surfactant composites were prepared from MMSS n by the SE method.⁽¹⁶⁾ 1 g of MMSS18 silica/surfactant composite powder was added to 60 mL of 0.1 M $C_{22}\text{TMACl}$ solution in ethanol–water (50:50 v/v). The suspension was sealed and placed in an oven at 100°C for 7 days without stirring. The resultant white powder was filtered, washed with distilled water and dried. The powder was calcined in air at 550°C for 6 h to remove organic species. Hereafter, the samples obtained by the SE method are denoted as PS(22)MS18.

2.4 Pore Expansion of MMSS18 by the SI Method

In the SI method,⁽¹⁷⁾ hydrophobic reagents such as TMB, 1,3,5-triisopropylbenzene, anthracene, 1,10-phenanthroline, benzene, cyclohexane, dodecane, hexane, or naphthalene were used. 1 g of MMSS18 silica/surfactant composite was added to 60 mL of an ethanol–water (50:50 v/v) solution including 2.25 g of a swelling agent. The subsequent steps were the same as those for the SE method, but the resulting white powder was washed with ethanol or an ethanol/water mixture instead of water. The powder was calcined in air at 550°C for 6 h to remove any remaining organic species. The samples obtained by the SI method are denoted as PS(sa)MS18 (“sa” represents the swelling agent used for the treatment) hereafter. Incorporation of TMB was also conducted with a 0.1 M $C_{22}\text{TMACl}$ ethanol–water (50:50 v/v) solution. The sample

obtained with this procedure is denoted as PS(22, TMB)MS18.

2.5 Synthesis of Monodispersed Porous Ferromagnetic Composite Spheres

$\text{Fe}(\text{NO}_3)_3 \cdot 9\text{H}_2\text{O}$ and $\text{H}_2\text{PtCl}_6 \cdot 6\text{H}_2\text{O}$ were used as metal sources. In a typical synthesis, the (pore-expanded) MMSS were impregnated with an aqueous solution containing $\text{Fe}(\text{NO}_3)_3$ and H_2PtCl_6 (Si:Fe:Pt = 84:8:8 molar ratio) and the mixture was evaporated until dry. The yellow powder obtained was calcined at 800°C for 4 h under a reducing atmosphere ($\text{N}_2:\text{H}_2 = 95:5$ v/v). Reduction was conducted at a higher temperature (usually 600°C for bulky FePt), considering the difficulty of FePt crystallization inside the mesopores.

2.6 Characterization

Scanning electron microscopy (SEM; SIGMA-V, Akashi Seisakusyo), energy-dispersive X-ray spectroscopy (EDX; S-3600N, Hitachi High-Technologies Corporation) and transmission electron microscopy (TEM; JEM2000EX, JEOL) were used to characterize the particle size, morphology and the elemental composition. The average particle size and standard deviation were estimated using 50 particles in each SEM image. Thermal desorption system-gas chromatography/mass spectrometry (TDS-GC/MS; GC6890/5973N, Agilent Technologies) was used to analyze TMB in the sample. The surfactants in the composite were analyzed by electrospray ionization mass spectrometry (ESI-MS; Q-TOF, Micromass) and matrix-assisted laser desorption/ionization time-of-flight mass spectrometry (MALDI-TOF/MS; Autoflex, Bruker Daltonics). The constituent phases were determined by X-ray diffraction (XRD; RINT 2200, Rigaku) analysis using $\text{Cu K}\alpha$ radiation. Magnetic properties were measured at room temperature with a vibrating sample magnetometer (VSM-3S-15, Toei Industry). The pore properties were determined by nitrogen adsorption-desorption analysis (BELSORP-mini II, BEL Japan). The specific surface areas were obtained using the Brunauer, Emmett, and Teller (BET) multimolecular layer adsorption model, and the average pore diameters were calculated from the desorption branch using the Barrett, Joyner, and Halenda (BJH) model.

3. Results and Discussion

3.1 Pore Expansion of MMSS by the SE Method

SEM and TEM images of PS(22)MS18 produced from the solvothermal treatment of MMSS18 with $\text{C}_{22}\text{TMACl}$ are shown in **Fig. 1**(a) and (c), respectively. MMSS n and PS(22)MS n particles both retained high monodispersity and spherical morphology after solvothermal treatment. The coefficients of variation for the average diameters were less than 10%. The mesopores in PS(22)MS10 are aligned radially from the center to the outside of the spherical particles, as shown in **Fig. 1**(c).

The XRD patterns of MMSS n and PS(22)MS n (not shown) have (100) diffraction peaks at $2\theta = 2.59\text{--}3.41^\circ$ and $1.65\text{--}2.22^\circ$, respectively, which indicate the presence of an ordered mesoporous structure. The d_{100} values calculated from 2θ are 2.59–3.41 nm and 3.98–5.35 nm, respectively, which confirms that hydrothermal treatment led to enlargement of the unit-cells.

The nitrogen adsorption-desorption isotherms and the corresponding pore size distributions of MMSS n and PS(22)MS n are shown in **Fig. 2**. The isotherms are type IV curves. MMSS n and PS(22)MS n exhibit reversible adsorption-desorption isotherms without hysteresis, and the volume adsorbed was $270\text{--}560\text{ cm}^3$ (STP) g^{-1} and $660\text{--}820\text{ cm}^3$ (STP) g^{-1} , respectively. The corresponding pore size distributions are very narrow, as shown in **Fig. 2**(b). The particle characteristics for MMSS n and PS(22)MS n are summarized in **Table 1**. The pore diameters and volumes increased

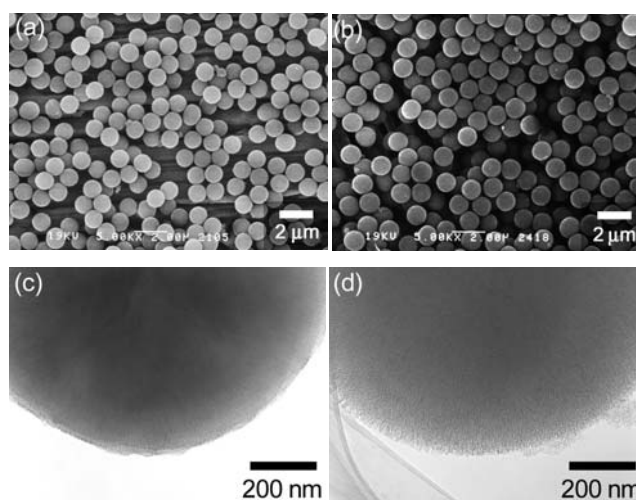


Fig. 1 SEM and TEM images of pore-expanded MMSS samples; (a, c) PS(22)MS18, (b, d) PS(TMB)MS18.

substantially, up to 2.8 and 2.4 times larger than the original values, respectively, while retaining high surface areas and narrow pore size distributions.

The d_{100} spacing and the average pore diameter of MMSS n increased with n , according to the alkyl-chain length of the surfactant. However, the equivalent values for PS(22)MS n were slightly decreased. The regularity of mesopores in MMSS n was higher when a surfactant with a longer alkyl-chain was used. It is assumed that reorganization of the mesopores tends to occur more easily in mesoporous silicas with less regularity.

When swelling agents are used, the pores should be expanded by the introduction of these molecules to the surfactants inside the mesopores. If C₂₂TMA surfactants are introduced into the mesopores of MMSS n , both C₂₂ and C_{*n*}TMA surfactants should be detected in PS(22)MS n . The surfactants inside PS(22)MS n prior to calcination were analyzed by

ESI-MS and MALDI-TOF/MS. The MALDI-TOF/MS spectra of PS(22)MS n and the ESI-LC/MS spectra (not shown) of the surfactant extracted from PS(22)MS n show only a dehalogenated C₂₂-TMA peak ($m/z = 368.4$). In addition, the organic content of MMSS n was significantly increased after pore-expansion. The organic contents of MMSS n ($n = 10, 14, 18$) were 33.4, 43.4 and 51.0 wt%, respectively, while those of the corresponding PS(22)MS n increased to 47.2, 52.8 and 55.2 wt%, respectively.

These results also suggest that the surfactants inside the mesopores are completely exchanged for the longer alkyl-chain length surfactants, which would result from strong hydrophobic interaction between surfactants with longer alkyl-chain lengths. When identical numbers of surfactants with shorter alkyl-chain lengths are replaced by surfactants with longer alkyl-chain lengths, the pore diameters of the mesoporous silica should be increased.

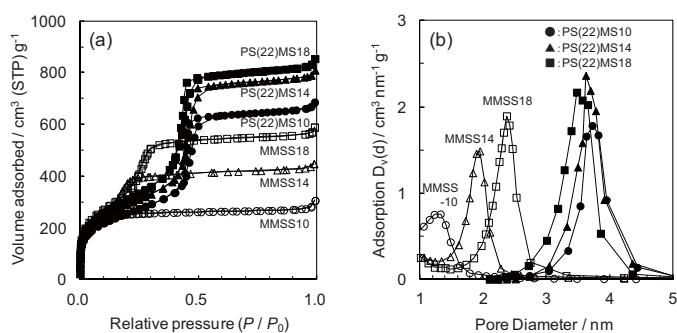


Fig. 2 (a) Nitrogen adsorption-desorption isotherms and (b) pore size distributions of MMSS n and PS(22)MS n .

3.2 Pore Expansion of MMSS by the SI Method

In the SE method, the use of ethanol-water solution led to unique pore expansion by control of the amount of silica dissolution. We have applied this method with a swelling agent such as TMB instead of C₂₂TMACl in the SI method, and mesopores of MMSS18 were expanded up to 2.2 times the original size. SEM and TEM images of PS(TMB)MS18 are shown in Figs. 1(b) and (d), and a summary of the particle characteristics are listed in **Table 2**. PS(TMB)MS18 retained highly uniform spherical morphology, as

Table 1 Particle characteristics of MMSS n and PS(22)MS n .

Sample	Average diameter / μm	Coefficient of variation /%	d_{100} /nm	Specific surface area / $\text{m}^2 \text{g}^{-1}$	Average pore size /nm	Pore volume / $\text{cm}^3 \text{g}^{-1}$
MMSS10	786	6.0	2.59	878	1.33	0.42
MMSS14	626	8.6	3.14	1179	1.96	0.66
MMSS18	836	4.3	3.41	1245	2.38	0.86
PS(22)MS10	887	5.5	5.35	934	3.73	1.01
PS(22)MS14	617	7.3	4.72	1058	3.63	1.20
PS(22)MS18	793	5.0	3.98	1130	3.49	1.27

Table 2 Particle characteristics of MMSS18 and pore-expanded MMSS18 samples.

Sample	Average diameter / μm	Coefficient of variation /%	d_{100} /nm	Specific surface area / $\text{m}^2 \text{g}^{-1}$	Average pore size /nm	Pore volume / $\text{cm}^3 \text{g}^{-1}$
MMSS18	1.17	4.4	3.61	1240	2.46	0.95
PS(22)MS18	1.10	4.4	4.02	1120	3.58	1.13
PS(TMB)MS18	1.19	3.8	6.96	910	5.46	1.66

shown in Fig. 1(b). The average diameters of MMSS18 and PS(TMB)MS18 were 1.17 and 1.19 μm , which varied only slightly after post-solvothermal treatment. Moreover, TEM images indicated that radial alignment of mesopores was retained after reorganization of the mesopores during pore expansion.

The XRD pattern of PS(TMB)MS18 (not shown) has (100) diffraction peaks at $2\theta = 1.27^\circ$, which indicates an ordered mesoporous structure. The d_{100} value calculated from 2θ was 6.96 nm. The nitrogen adsorption-desorption isotherms and the corresponding pore size distributions for PS(TMB)MS18 are shown in Fig. 3. The isotherm is a type IV curve; a reversible adsorption-desorption isotherm was observed with a characteristic nitrogen condensation-evaporation step at a relative pressure of ca. 0.6, and the volume adsorbed was 1,075 cm^3 (STP) g^{-1} . Fig. 3(b) shows sharp pore size distribution curves for the samples before and after solvothermal treatment.

When the solvothermal treatment of MMSS was conducted in the presence of both $\text{C}_{22}\text{TMACl}$ and TMB, the pore diameter of PS(22,TMB)MS18 was expanded to 4.24 nm, which was smaller than that of PS(TMB)MS18. In a solution with surfactants present, the solubility of TMB probably increases to form a micelle. It is assumed that this increase in solubility causes a decrease in the amount of TMB incorporated into hydrophobic surfactant micelles inside mesopores. It was confirmed that mesopores could be significantly expanded by the SI method. An investigation was then conducted to clarify those types of swelling agents that could satisfactorily expand the mesopores. Table 3 lists the particle characteristics of the PS(sa)MS18 samples.

The use of tricyclic agents, such as anthracene and 1,10-phenanthroline, resulted in lower pore expansion,

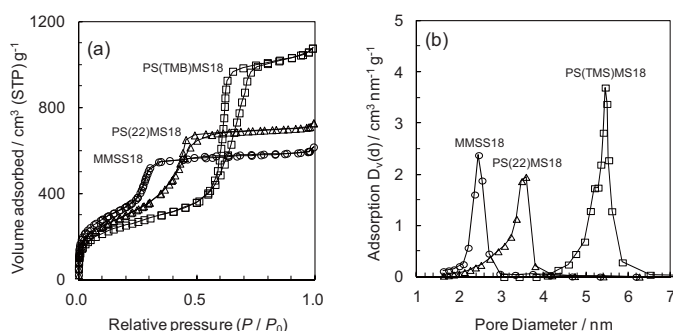


Fig. 3 (a) Nitrogen adsorption-desorption isotherms and (b) pore size distributions of MMSS18 and pore-expanded MMSS18 samples.

because their larger molecular sizes prevented incorporation into the micelle rods inside the mesopores. In contrast, the pores were more effectively expanded using smaller sized molecules, of which TMB was the most effective expanding agent. A water-ethanol solution was used as the solvent in the SI method, and reagents with higher affinity for the solvent are expected to increase their distribution in the solvent, but decrease that in the hydrophobic micelle rods. Therefore, it would be concluded that appropriately sized hydrophobic reagents are effective as swelling agents, except *N, N*-dimethyldecylamine (DMDA). Although the solubility of DMDA in the water-ethanol mixed solvent is higher, this agent had the next best effect for pore expansion after TMB. It has been proposed that the alkylamine is self-assembled into an inverted cylindrical micelle inside the alkyltrimethylammonium micelle in the presence of water, being held via attractive hydrophobic forces.⁽¹¹⁾ Therefore, it is likely that the mechanism of pore expansion using DMDA is different from that for the other hydrophobic reagents.

If TMB is incorporated into the mesopores of MMSS n , then TMB should be detected in PS(TMB)MS18. The TMB inside the PS(TMB)MS18 prior to calcination was analyzed by TDS-GC/MS. The TDS-GC/MS spectrum (not shown) of PS(TMB)MS18 has a TMB peak ($m/z = 120$), which confirms that the TMB in solution had been incorporated into the mesopores of MMSS. It is assumed that a strong hydrophobic interaction between the surfactant alkyl

Table 3 Particle characteristics of MMSS18 and pore-expanded MMSS18 samples.

Sample	Specific surface area / $\text{m}^2 \text{g}^{-1}$	Average pore size / nm	Pore volume / $\text{cm}^3 \text{g}^{-1}$
Original MMSS-18	1240	2.46	0.95
PS(Anthracene)MS18	1130	3.04	1.09
PS(1,10-Phen)MS18 ^a	1110	3.06	1.06
PS(Benzene)MS18	1110	3.27	1.11
PS(TiPB)MS18 ^b	1000	3.72	1.40
PS(Cyclohexane)MS18	1110	3.91	1.20
PS(Dodecane)MS18	1120	3.99	1.48
PS(Hexane)MS18	1150	4.55	1.50
PS(Naphthalene)MS18	1050	5.03	1.21
PS(DMDA)MS18 ^c	1070	5.16	1.84
PS(TMB)MS18	910	5.46	1.66

^a 1,10-Phenanthroline. ^b TiPB: 1,3,5-Triisopropylbenzene.
^c DMDA: *N, N*-Dimethyldecylamine.

chain and TMB leads to this incorporation. The pore diameters of the mesoporous silica should increase once TMB is incorporated into the mesopores. The reorganization of the mesopores of MMSS by dissolution and redeposition of silica components leads to the pore expansion of MMSS as illustrated in Fig. 4.

3.3 FePt-MMSS Composites

Highly monodispersed superparamagnetic composite spheres have been successfully synthesized by incorporating iron oxides such as γ -Fe₂O₃ and ϵ -Fe₂O₃ into MMSS16.⁽¹⁸⁾ The next target was to prepare a monodispersed ferromagnetic composite. These iron oxide particles must be greater than 10 nm to exhibit ferromagnetism (threshold size); therefore, the goal was to incorporate FePt nanoparticles with smaller threshold sizes (2.8–3.3 nm) to realize ferromagnetism in MMSS.⁽¹⁹⁾ Figs. 5(a)–(c) show SEM images of FePt-MMSS composite particles. Some FePt nanoparticles were observed on the surface of the FePt-MMSS18 composite; however, no small particles were observed on the outer surfaces of the FePt-PS(22)MS18 and

FePt-PS(TMB)MS18 composites, which suggests that the large mesopores of MMSS play a key role in keeping the FePt nanoparticles inside MMSS. The Fe/Pt ratio determined from EDX analysis was ca. 0.45 for all composites.

Table 4 lists the particle characteristics of the FePt-MMSS composites. The specific surface area, average pore diameter, and pore volume of these composites decreased compared with those of MMSS (Table 1). However, the FePt-MMSS composites adsorbed a certain amount of nitrogen, of which FePt-PS(TMB)MS18 had the largest pore volume (0.74 cm³ g⁻¹), which is still sufficient to incorporate other chemicals, nanoparticles, proteins, quantum dots, and enzymes.

TEM images of FePt-MMSS composites are shown in Figs. 5(d)–(f). It is confirmed the FePt nanoparticles are present in the internal structures of the composites; FePt nanoparticles incorporated in the mesopores are indicated by black dots in the micrographs, and the mesopores are aligned radially from the center to the outside of the spherical particles in all the composite particles.



Fig. 4 Schematic representation of MMSS pore expansion.

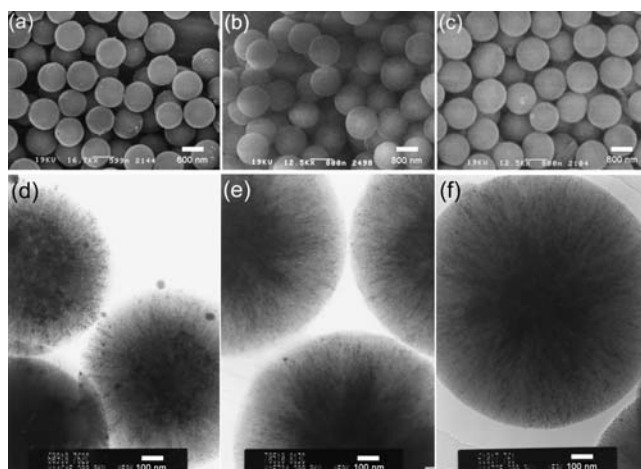


Fig. 5 SEM and TEM images of FePt-MMSS composites: (a, d) FePt-MMSS18, (b, e) FePt-PS(22)MS18, and (c, f) FePt-PS(TMB)PS18.

Table 4 Particle Characteristics of FePt Composites.

Sample	Specific surface area /m ² g ⁻¹	Average pore size /nm	Pore volume /cm ³ g ⁻¹
FePt-MMSS18	810	2.14	0.50
FePt-PS(22)MS18	680	3.28	0.56
FePt-PS(TMB)MS18	580	4.54	0.74

The XRD patterns of the composite particles match the pattern for tetragonal FePt (JCPDS 65-9121). The broad XRD peaks should be attributed to nanometer sized FePt particles; however, in the pattern of FePt-MMSS18, sharp peaks overlap with broader peaks. These sharp peaks are assignable to larger FePt nanoparticles formed outside the composite, as evident in the SEM and TEM images. Assuming that the FePt nanoparticles are spherical, the average diameters were calculated using the Scherrer equation to be 4.1 and 5.5 nm for FePt-PS(22)MS18 and FePt-PS(TMB)MS18 composites, respectively.⁽²⁰⁾ These values correlate well with the average pore sizes of PS(22)MS18 (3.6 nm) and PS(TMB)MS18 (5.5 nm). It is assumed that some mesopores were collapsed by the growth of FePt nanoparticles when the mesopore size was not sufficiently large. From these results, it was concluded that the particle size of FePt could be controlled by varying the size of the mesopores in MMSS.

Both FePt-PS(22)MS18 and FePt-PS(TMB)MS18 were expected to exhibit ferromagnetic behavior, because the sizes of the FePt nanoparticles inside the mesopores were larger than the threshold size for ferromagnetism.⁽¹⁹⁾ Magnetization curves for FePt-MMSS18, FePt-PS(22)MS18, and FePt-PS(TMB)MS18 are shown in **Fig. 6**. A hysteresis loop was observed in each curve by the ferromagnetic behavior of FePt nanoparticles in the composites; however, a decrease in the magnetization around zero magnetic fields suggests the existence of superparamagnetic components. The coercivities of FePt-PS(22)MS18

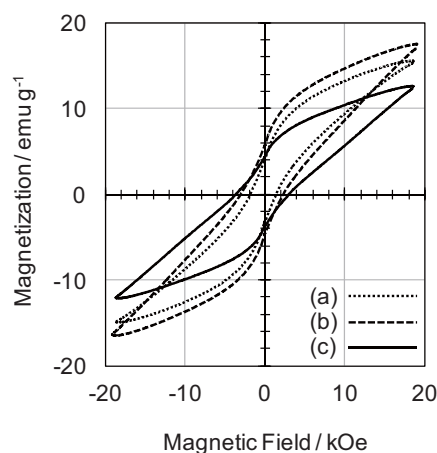


Fig. 6 Magnetization curves of FePt-MMSS composites: (a) FePt-MMSS18, (b) FePt-PS(22)MS18, and (c) FePt-PS(TMB)MS18.

and FePt-PS(TMB)MS18 were 2.7 and 3.3 kOe, respectively. The pore diameter of MMSS18 is much smaller than the threshold size of ferromagnetism for FePt nanoparticles; however, a hysteresis loop was observed in the curve for FePt-MMSS18. The FePt nanoparticles outside MMSS (Fig. 5) probably contributed to the ferromagnetism of FePt-MMSS18. The coercivities of the composites correspond well to the sizes of the FePt nanoparticles, which were calculated using the Scherrer equation.

4. Conclusions

In conclusion, pore expansion of monodispersed mesoporous silica spheres (MMSS) was conducted using the SE and SI methods. The pore diameter was expanded up to 3.7 and 5.5 nm using the SE and SI methods, respectively, while retaining the morphology, monodispersity and radially, hexagonally-ordered mesopores. This was achieved by solvothermal treatment of MMSS in an ethanol-water mixed solvent system. In the SE method, the C₂₂TMACl surfactant with a longer alkyl-chain length was used and the surfactants inside the mesopores were completely exchanged for the C₂₂TMACl surfactant. The driving force for surfactant exchange is the strong hydrophobic interaction between the longer alkyl-chains of C₂₂TMACl. In contrast, hydrophobic swelling agents, such as TMB, were used for the SI method. The swelling agent penetrated into the micelle rods inside the mesopores by hydrophobic interaction between the alkyl-chains of the surfactants and the swelling agent. Highly monodispersed ferromagnetic composite spheres were successfully obtained using pore-expanded MMSS. When large pore diameter MMSS were used, FePt nanoparticles were uniformly dispersed in the mesopores without deposition on the surface of MMSS. These composites have both ferromagnetic behavior at room temperature and mesoporosity with a large pore volume.

Application of these methods enables control of the pore diameter, particle size, and amount of FePt nanoparticles in the FePt-MMSS composites. The composites still have large surface areas and pore volumes, so that a variety of nanoparticles, quantum dots, enzymes, and DNA molecules, can be further incorporated into the mesopores. These methods have potential applications in drug delivery systems, gene delivery systems, magnetic hyperthermia devices, and magnetic photonic crystals.

Acknowledgment

This research was partly supported by a Grant-in-Aid for Scientific Research (B, 17310079, 2006) from the Japan Society for the Promotion of Science (JSPS). The authors received technical assistance from Kazuo Okamoto (MALDI-TOF/MS), Ayako Ohshima (TDS-GC/MS), Yusuke Akimoto (TEM), and Shuji Kajiya (ESI-MS).

References

- (1) (a) Kresge, C. T., Leonowicz, M. E., Roth, W. J., Vartuli, J. C. and Beck, J. S., "Ordered Mesoporous Molecular Sieves Synthesized by a Liquid-crystal Template Mechanism", *Nature*, Vol.359, No.6397 (1992), pp.710-712. (b) Beck, J. S., Vartuli, J. C., Roth, W. J., Leonowicz, M. E., Kresge, C. T., Schmitt, K. D., Chu, C. T-W., Olson, D. H., Sheppard, E. W., McCullen, S. B., Higgins, J. B. and Schlenker, J. L., "A New Family of Mesoporous Molecular Sieves Prepared with Liquid Crystal Templates", *J. Am. Chem. Soc.*, Vol.114, No.27 (1992), pp.10834-10843.
- (2) (a) Sayari, A., "Catalysis by Crystalline Mesoporous Molecular Sieves", *Chem. Mater.*, Vol.8, No.8 (1996), pp.1840-1846. (b) Taguchi, A. and Schüth, F., "Ordered Mesoporous Materials in Catalysis", *Microporous Mesoporous Mater.*, Vol.77, No.1 (2005), pp.1-45. (c) Hoffmann, F., Cornelius, M., Morell, J. and Fröba, M., "Silica-based Mesoporous Organic-inorganic Hybrid Materials", *Angew. Chem., Int. Ed.*, Vol.45, No.20 (2006), pp.3216-3251.
- (3) (a) Maschmeyer, T., Rey, F., Sankar, G. and Thomas, J. M., "Heterogeneous Catalysts Obtained by Grafting Metallocene Complexes onto Mesoporous Silica", *Nature*, Vol.378, No.6553 (1995), pp.159-162. (b) Reynhardt, J. P. K., Yang, Y., Sayari, A. and Alper, H., "Periodic Mesoporous Silica-supported Recyclable Rhodium-complexed Dendrimer Catalysts", *Chem. Mater.*, Vol.16, No.21 (2004), pp.4095-4102.
- (4) (a) Antochshuk, V., Olkhoviyk, O., Jaroniec, M., Park, I. S. and Ryoo, R. "Benzoylthiourea-modified Mesoporous Silica for Mercury(II) Removal", *Langmuir*, Vol.19, No.7 (2003), pp.3031-3034. (b) Kang, T., Park, Y., Choi, K., Lee, J. S. and Yi, J., "Periodic Mesoporous Silica-supported Recyclable Rhodium-complexed Dendrimer Catalysts", *J. Mater. Chem.*, Vol.14, No.6 (2004), pp.1043-1049.
- (5) (a) Benitez, M., Bringmann, G., Dreyer, M., Garcia, H., Ihmels, H., Waidelich, M. and Wissel, K., "Design of a Chiral Mesoporous Silica and Its Application as a Host for Stereoselective di-p-methane Rearrangements", *J. Org. Chem.*, Vol.70, No.6 (2005), pp.2315-2321. (b) Tura, C., Coombs, N. and Dag, O., "One-Pot Synthesis of CdS Nanoparticles in the Channels of Mesostructured Silica Films and Monoliths", *Chem. Mater.*, Vol.17, No.3 (2005), pp.573-579.
- (6) Stöber, W., Fink, A. and Bohn, E., "Controlled Growth of Monodisperse Silica Spheres in the Micron size range", *J. Colloid Interface Sci.*, Vol.26, No.1 (1968), pp.62-69.
- (7) (a) Grün, M., Büchel, G., Kumar, D., Schumacher, K., Bidlingmaier, B. and Unger, K. K., "Rational Design, Tailored Synthesis and Characterization of Ordered Mesoporous Silicas in the Micron and Submicron Size Range", *Stud. Surf. Sci. Catal.*, Vol.128 (2000), pp.155-165. (b) Grün, M., Lauer, I. and Unger, K. K., "The Synthesis of Micrometer- and Submicrometer-size Spheres of Ordered Mesoporous Oxide MCM-41", *Adv. Mater.*, Vol.9, No.3 (1997), pp.254-257. (c) Schumacher, K., Renker, S., Unger, K. K., Ulrich, R., Chesne, A. D., Spiess, H. W. and Wiesner, U., "A Novel Approach to Polymer-template Mesoporous Molecular Sieves", *Stud. Surf. Sci. Catal.*, Vol.129 (2000), pp.1-6. (d) Luo, Q., Li, L., Xue, Z. and Zhao, D., "Synthesis of Nanometer-sized Mesoporous Silica and Alumina Spheres", *Stud. Surf. Sci. Catal.*, Vol.129 (2000), pp.37-43.
- (8) (a) Yano, K., Suzuki, N., Akimoto, Y. and Fukushima, Y., "Synthesis of Mono-dispersed Mesoporous Silica Spheres with Hexagonal Symmetry", *Bull. Chem. Soc. Jpn.*, Vol.75, No.9 (2002), pp.1977-1982. (b) Yano, K. and Fukushima, Y., "Particle Size Control of Mono-dispersed Super-microporous Silica Spheres", *J. Mater. Chem.*, Vol.13, No.10 (2003), pp.2577-2581.
- (9) Yamada, Y., Nakamura, T., Ishii, M. and Yano, K., "Reversible Control of Light Reflection of a Colloidal Crystal Film Fabricated from Monodisperse Mesoporous Silica Spheres", *Langmuir*, Vol.22, No.6, pp.2444-2446.
- (10) Yano, K. and Fukushima, Y., "Synthesis of Mono-dispersed Mesoporous Silica Spheres with Highly Ordered Hexagonal Regularity Using Conventional Alkyltrimethylammonium Halide as a Surfactant", *J. Mater. Chem.*, Vol.14, No.10 (2004), pp.1579-1584.
- (11) (a) Lefèvre, B., Galarneau, A., Iapichella, J., Petitto, C., Renzo, F. D., Fajula, F., Bayram-Hahn, Z., Skudas, R. and Unger, K., "Synthesis of Large-pore Mesostructured Micelle-templated Silicas as Discrete Spheres", *Chem. Mater.*, Vol.17, No.3 (2005), pp.601-607. (b) Pauly, T. R. and Pinnavaia, T. J., "Pore Size Modification of Mesoporous HMS Molecular Sieve Silicas with Wormhole Framework Structures", *Chem. Mater.*, Vol.13, No.3 (2001), pp.987-993. (c) Kimura, T., Sugahara, Y. and Kuroda, K., "Synthesis of Mesoporous Aluminophosphates Using Surfactants with Long Alkyl Chain Lengths and Triisopropylbenzene as a Solubilizing Agent", *Chem.*

- Commun.*, Vol.34, No.5 (1998), pp.559-560.
- (d) Ulagappan, N. and Rao, C. N. R., "Evidence for Supramolecular Organization of Alkane and Surfactant Molecules in the Process of Forming Mesoporous Silica", *Chem Commun.*, Vol.32, No.24 (1996), pp.2759-2760. (e) Zhang, W., Pauly, T. R. and Pinnavaia, T. J., "Tailoring the Framework and Textural Mesopores of HMS Molecular Sieves through an Electrically Neutral ($S^{\circ}P^{\circ}$) Assembly Pathway", *Chem. Mater.*, Vol.9, No.11 (1997), pp.2491-2498.
- (12) (a) Hanrahan, J. P., Copley, M. P., Ryan, K. M., Spalding, T. R., Morris, M. A. and Holmes, J. D., "Pore Expansion in Mesoporous Silicas Using Supercritical Carbon Dioxide", *Chem. Mater.*, Vol.16, No.3 (2004), pp.424-427. (b) Sayari, A., Hamoudi, S. and Yang, Y., "Applications of Pore-expanded Mesoporous Silica. 1. Removal of Heavy Metal Cations and Organic Pollutants from Wastewater", *Chem. Mater.*, Vol.17, No.1 (2005), pp.212-216. (c) Sun, J.-H. and Coppens, M.-O., "A Hydrothermal Post-synthesis Route for the Preparation of High Quality MCM-48 Silica with a Tailored Pore Size", *J. Mater. Chem.*, Vol.12, No.10 (2002), pp.3016-3020. (d) Sayari, A., Kruk, M., Jaroniec, M. and Moudrakovski, I. L., "New Approaches to Pore Size Engineering of Mesoporous Silicates", *Adv. Mater.*, Vol.10, No.16 (1998), pp.1376-1379. (e) Sun, J.-H. and Coppens, M.-O., "Alcothermal Synthesis of Large Pore, High Quality MCM-48 Silica", *Stud. Surf. Sci. Catal.*, Vol.141 (2002), pp.85-92.
- (13) Klemmer, T., Hoydick, D., Okumura, H., Zhang, B. and Soffa, W. A., "Magnetic Hardening and Coercivity Mechanisms in L1o Ordered FePd Ferromagnets", *Scr. Met. Mater.*, Vol.33, No.10-11 (1995), pp.1793-1805.
- (14) Sun, S., "Recent Advances in Chemical Synthesis, Self-assembly, and Applications of FePt Nanoparticles", *Adv. Mater.*, Vol.18, No.4 (2006), pp.393-403.
- (15) (a) Takahashi, Y. K., Ohkubo, T., Ohnuma, M. and Hono, K., "Size Effect on the Ordering of FePt Granular Films", *J. Appl. Phys.*, Vol.93, No.10 (2003), pp.7166-7168. (b) Takahashi, Y. K., Koyama, T., Ohnuma, M., Ohkubo, T. and Hono, K., "Size Dependence of Ordering in FePt Nanoparticles", *J. Appl. Phys.*, Vol.95, No.5 (2004), pp.2690-2696.
- (16) Mizutani, M., Yamada, Y. and Yano, K., "Pore-expansion of Monodisperse Mesoporous Silica Spheres by a Novel Surfactant Exchange Method", *Chem. Commun.*, Vol.43, No.11 (2007), pp.1172-1174
- (17) Mamoru, M., Yuri, Y., Tadashi N. and Kazuhisa, Y., "Anomalous Pore Expansion of Highly Monodispersed Mesoporous Silica Spheres and Its Application to the Synthesis of Porous Ferromagnetic Composite", *Chem. Mater.*, Vol.20, No.14 (2008), pp.4777-4782.
- (18) Nakamura, T., Yamada, Y. and Yano, K., "Novel Synthesis of Highly Monodispersed γ -Fe₂O₃/SiO₂ and ϵ -Fe₂O₃/SiO₂ Nanocomposite Spheres", *J. Mater. Chem.*, Vol.16, No.25 (2006), pp.2417-2419.
- (19) Weller, D., Moser, A., Folks, L., Best, M. E., Lee, W., Toney, M. F., Schwickert, M., Thiele, J.-U. and Doerner, M. F., "High K_u Materials Approach to 100 Gbits/in²", *IEEE Trans. Magn.*, Vol.36, No.1 (2000), pp.10-15.
- (20) Scherrer, P., "Bestimmung der Grösse und der Inneren Struktur von Kolloidteilchen Mittels Röntgenstrahlen", *Nachrichten von der Gesellschaft der Wissenschaften zu Göttingen, Mathematisch-Physikalische Klasse* (1918), pp.98-100.

Figs. 1, 3-6 and Tables 2-4

Reprinted from *Chem. Mater.*, Vol.20, No.14 (2008), pp.4777-4782, Mizutani, M., Yamada, Y., Nakamura, T. and Yano, K., Anomalous Pore Expansion of Highly Monodispersed Mesoporous Silica Spheres and Its Application to the Synthesis of Porous Ferromagnetic Composite, © 2008 ACS, with permission from American Chemical Society.

Fig. 2 and Table 1

Reprinted from *Chem. Commun.*, Vol.43, No.11 (2007), pp.1172-1174, Mizutani, M., Yamada, Y. and Yano, K., Pore-expansion of Monodisperse Mesoporous Silica Spheres by a Novel Surfactant Exchange Method., © 2007 The Royal Society of Chemistry.

Mamoru Mizutani

Research Fields:

- Lithium-ion Secondary Battery
- Materials Chemistry

Academic Degree: Dr. Eng.

Academic Society:

- The Chemical Society of Japan



Yuri Yamada

Research Fields:

- Inorganic Materials Chemistry
- Coating Technology

Academic Degree: Dr. Eng.

Academic Societies:

- The Chemical Society of Japan
- American Chemical Society



Tadashi Nakamura

Research Fields :

- Inorganic Materials Chemistry
- Solid State Electrochemistry

Academic Degree : Dr. Eng.

Academic Societies :

- The Chemical Society of Japan
- The Ceramic Society of Japan
- The Electrochemical Society of Japan

Award :

- Award of the Outstanding Papers Published in the JCSJ in 2004, 2005

**Kazuhisa Yano**

Research Fields :

- Porous Materials
- Colloidal Crystals

Academic Degree : Dr. Eng.

Academic Society :

- American Chemical Society

